metals

MDPI

Article

Quality Diagnostics of Parts Produced by Combined Additive Manufacturing Technology

Alexander S. Metel, Tatiana Tarasova *, Andrey Skorobogatov, Pavel Podrabinnik, Marina Volosova and Sergey N. Grigoriev

Department of High-Efficiency Machining Technologies, Moscow State University of Technology "STANKIN", Vadkovsky Lane 3a, 127055 Moscow, Russia

* Correspondence: tarasova952@mail.ru

Abstract: The work is focused on the combined process of obtaining bimetallic parts that involve laser-directed energy deposition (LDED) additive technology and the conventional casting process. In this research, molybdenum powder was deposited by LDED on a cast 25L steel substrate. The choice of materials is motivated by demands for replacing the traditional technique of brazing molybdenum with a copper interlayer on low-carbon steel to eliminate shortcomings. The influence of powder particle morphology on the quality of deposited layers was studied. Spherical molybdenum powder PMS-M99.9 facilitated stable deposition of good layers and was found to be suitable for the LDED. Quality diagnostics were performed by studying microstructure, hardness, and wear resistance properties. Preferential parameters of the LDED of molybdenum were found through parametrical analysis. Microstructural studies showed that LDED of PMS-M99.9 powder results in a homogeneous stable layer with a strong bond to the steel substrate, which was confirmed by mutual diffusion of Mo and Fe in the boundary. It is also demonstrated that the found working parameters of LDED assure high hardness, wear, and fretting wear resistance. The three studied coatings (LDED of powders PMS-M99.9 and PM-M; VM1 brazing) had the same friction coefficient value of ~0.25. Compared to others, PMS-M99.9 coating had the lowest volumetric wear, while abrasive wear was measured to be the highest.

Keywords: laser-directed energy deposition; additive technologies; multimaterial objects; bimetals; steel; nickel alloy; molybdenum; powder; wear resistance; fretting

Citation: Metel, A.S.; Tarasova, T.; Skorobogatov, A.; Podrabinnik, P.; Volosova, M.; Grigoriev, S.N. Quality Diagnostics of Parts Produced by Combined Additive Manufacturing Technology. *Metals* **2023**, *13*, 19. https://doi.org/10.3390/met13010019

Academic Editor: Pavel Krakhmalev

Received: 7 November 2022
Revised: 8 December 2022
Accepted: 17 December 2022
Published: 22 December 2022

1. Introduction

The development of modern industry in the direction of increasing the service life of components and mechanisms is inextricably linked with the development and improvement of processing technologies and the creation of new materials and methods for modifying surfaces. To increase the wear resistance of the surface of metallic materials, various methods are used (thermal, chemical–thermal, and mechanical). Laser hardening and cold gas dynamic spraying are among the most promising technologies [1–5]. As technological progress continues, industries demand more complex parts combining intricate shapes and advanced physical and chemical properties. A probable solution may be found in rapidly developing additive technologies (ATs) such as powder bed fusion using a laser beam (PBF-LB) and laser-directed energy deposition (LDED) [6–9].

The list of metal materials suitable for additive manufacturing (AM) is growing intensively. Furthermore, AM technologies for ceramics are also developing [10,11]. Special attention is paid to process diagnostics by determining the brightness temperature and restoring the true temperature in the laser exposure zone [12–15].

Using LDED technology, it is possible to manufacture products through a combined method, for example, to apply a deposited layer with the required performance characteristics to the surface of products on a workpiece made by casting or PBF-LB. Such bimetallic

products are in demand in modern industries; for example, in the aerospace industry, coatings that provide high wear resistance and withstand high operating temperatures are very common. However, for the practical application of LDED, it is necessary to carry out diagnostics of the quality of the resulting coatings, considering the operating conditions of the products. The quality criteria of the deposited coatings are flawless microstructure in the deposited layers, microhardness values, accuracy of the coating, wear resistance, and fretting wear behavior of the deposited layers.

Currently, in the field of development and research of the LDED technology to improve the performance of products, active research is being carried out by scientists from various international groups. Ding et al. [16] conducted comparative studies of the microstructure and properties of Inconel625 coatings on mild steel (27SiMn) obtained by ultra-high-speed laser cladding (UHSLC) and regular laser cladding (LSLC). It is reported that UHSLC has a cladding rate of 30 m/min which is 15 times higher than that of LSLC. As a result, the hardness, wear resistance, and corrosion resistance of Inconel625 coatings were greatly improved by increasing the speed of laser deposition.

With the development of aerospace technology and an increase in industrial production capacities, the temperatures of pre-turbine gases and the requirements for engine blade materials have increased [17–19].

Due to the limitation of the melting point, nickel-based superalloys cannot meet the urgent need to improve the performance of aircraft engines; thus, other types of high-temperature materials must be developed [20].

Mo-Si-B alloys are considered promising as high-temperature structural materials for next-generation aircraft engines and hypersonic vehicles due to their extremely high melting point (above 2000 °C), excellent heat resistance, good high-temperature oxidation resistance, and creep resistance [21].

The use of Mo-Si-B alloys will make it possible to increase the temperature of the pre-turbine gases of aircraft engines by 300–400 °C, which will significantly increase the efficiency of aircraft engines [22,23].

Laser-based AM technologies provide a high cooling rate while realizing a new way of three-dimensional shaping of Mo-Si-B alloys. Structures formed by LDED of Mo-Si-B alloys have higher oxidation resistance [24] and fracture toughness [25], indicating that AM is beneficial for this material. However, with Mo-Si-B alloys being very brittle, AM of Mo-Si-B alloys still faces significant challenges. Schmelzer et al. [26] were the first to publish successful results on probation Mo-Si-B alloys for LDED, reporting that they were able to obtain 3 mm of the deposited layer without cracks by induction heating of the substrate at 600 °C. It is noted that the microhardness of the layer was comparable to that of the cast alloy.

Zhou et al. [27,28] also successfully used the PBF-LB method for the three-dimensional molding of Mo-Si-B-Ti-C alloy powders prepared in a ball mill. Due to the fast solidification process, a fine-grained structure and uniform distribution of TiC nanoparticles were obtained, but the microhardness of the layer was lower than that of the cast alloy of the same composition due to the presence of microcracks inside the material.

Fichtner et. al. developed process parameters for LDED of Mo-Si-B alloys without cracks [29]. In [30], the Mo-Si-B alloy obtained by PBF-LB technology was studied, and the density and mechanical properties were determined at various process parameters and different ratios of the alloy components. It has been established that the Mo-Si-B alloy with the atomic composition (at.%) Mo (93.5), Si (4.5), and B (2.0), with a laser power of 250 W, scanning speed of 500 mm/s, and layer thickness of 60 microns, has the highest density value of 94.22 %.

Since pure molybdenum at room temperature is a brittle material, the authors studied the effect of Si and B additives on the bending strength. During the three-point bending experiment, it was found that the addition of elements Si and B gave the material some ductility, and the maximum bending force was 978.6 N. At present, studies of techno-

logical processes for the additive production of molybdenum-based alloys are still at the development stage and are not ready for wide practical use.

Due to the growing demands of the aerospace industry, there is also a need to develop a technology for the additive production of pure molybdenum on steel substrates [31]. In this regard, studies of PBF-LB of pure molybdenum are known [32]. The authors emphasize that the difficulties in obtaining a high-quality layer during PBF-LB are due to the high melting point of molybdenum and the high transition temperature of molybdenum from a plastic state to a brittle one. In the power density range from 0.44 J/mm to 0.64 J/mm, the authors managed to obtain even tracks with a small number of pores and microcracks. The maximum density of pure molybdenum obtained by PBF-LB molding was 99.1%.

The authors of [33] presented an overview of methods for obtaining multimaterial products, particularly via the LDED method. The prospects and problems of the methods are discussed. The main problems are the occurrence of defects in the deposited layers that occur at temperature gradients, as described in detail in [34].

The literature review showed that additive manufacturing of bimaterial objects is relevant and promising. However, at present, studies of AM processes of molybdenum-based alloys and studies in the field of LDED of pairs of materials such as molybdenum + low-carbon steel are still in the development stage and are not ready for industrial use.

This work is aimed at studying the LDED process of molybdenum on mild steel and diagnosing the quality of the deposited layers. In a previous study [31], the possibility of replacing the traditional technology of Mo soldering with carbon steel using copper solder with LDED was shown. In [31], the microstructure of brazed layers was studied, and the results were discussed. In the current work, the effect of powder morphology on the quality of the deposited layers is studied. Considering the operational requirements for the product, the structure, density, hardness, and wear resistance of the deposited coatings were studied.

2. Materials and Methods

2.1. Raw Materials

The choice of materials for the study was determined by the solution of a specific problem, which consists of replacing the traditional manufacturing technology of the bimetallic part "body" with a combined technology: conventional casting and LDED. The bimetallic part "body" is a body casting of steel grade 25L, to which a VM1 molybdenum plate is brazed with copper solder. It is designed to withstand high temperatures and maintain wear resistance. However, the working temperature may exceed the melting point of the copper solder leading to coating destruction. To tackle this problem, an alternative approach based on LDED of molybdenum powder on cast 25L substrate was proposed to exclude copper interlayer brazing. The chemical composition of the 25L steel is presented in Table 1.

Table 1. The chemical composition of the 25L steel substrate.

Material	Elements Composition, % Mass					
	Fe	**C**	**Mn**	**Si**	**S**	**P**
25L steel	Balance	0.30	0.54	0.51	0.019	0.024

Molybdenum powders PM-M (JSC "Polema", Tula, Russia) and PMS-M99.9 (JSC "Polema", Tula, Russia) of different morphology were used as raw materials in this study. The PM-M powder with irregularly shaped particles in the range of 20–63 μm was manufactured by mechanical disintegration. The PMS-M99.9 powder (particle size 40–100 μm) was produced by mechanical disintegration followed by plasma spheroidization. The chemical composition and properties of the raw powders are presented in Tables 2 and 3 correspondingly.

Table 2. The chemical composition of the Mo powders PMS-M99.9 and PM-M.

Material	Elements Composition, % Mass		
	Mo	Residual Elements [1], Total	O
PMS-M99.9	Balance	0.1	0.025
PM-M	Balance	0.2	0.025

[1] Al, Fe, K, Ca, Si, W, Mg, Ni, Na, Mn, and Zn.

Table 3. The properties of Mo powders PMS-M99.9 and PM-M.

Material	Flowability, s	Packed Density, g/cm^3	Tap Density, g/cm^3
PMS-M99.9	10.4	6.4	7.14
PM-M	n/a	3.96	5.3

To confirm the compliance of the raw powders with the required parameters specified in the standards for additive technologies [6,7], as well as to verify the parameters declared by the manufacturer, an input control of the powder materials was carried out. Granulometric analysis of powders was carried out on an Occhio 500 Nano optical morphometer (Occhio S.A., Liege, Belgium) with software for statistical image analysis (Figure 1). Morphological and elemental analyzes were performed on a Tescan Vega 3 LMH scanning electron microscope (SEM) (Tescan, Brno, Czech Republic) equipped with an energy-dispersive X-ray microanalyzer (Oxford Instruments, Abington, UK).

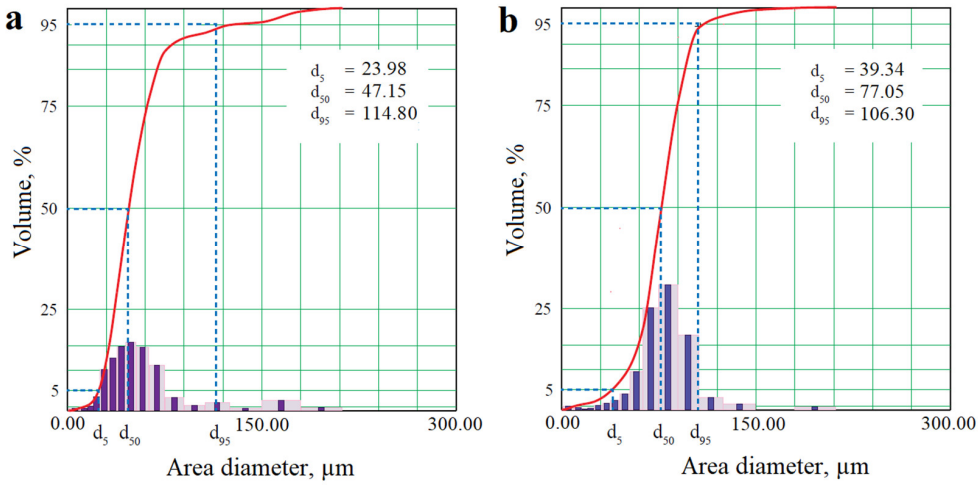

Figure 1. Integral curves and histograms of particle size distribution of powders: (**a**) PM-M; (**b**) PMS-M99.9.

The size distribution of powder particles is described by the Gaussian normal distribution law. It was found that the average particle size of the PM-M powder was d_{med} = 53.55 µm, and the volume of particles that did not correspond to the size of the main fraction declared by the manufacturer (from 20 to 63 µm) was 24.65%. The irregular shape of the particles was confirmed by SEM (Figure 2a). A high content of unintended fine particles affects negatively the flow focusing and makes it difficult to transport the powder to the nozzle. Therefore, the PM-M powder was sieved to meet the requirements for LDED powders.

The average particle size of the PMS-M99.9 powder was d_{med} = 76.79 µm, and the total content of particles that did not correspond to the size of the main fraction declared by the manufacturer (from 40 to 100 µm) was 9.75%. The shape of the powder particles was spherical with a high sphericity index of more than 90% (Figure 2b). The PMS-M99.9 powder was suitable for the LDED process; therefore, no additional sieving was performed.

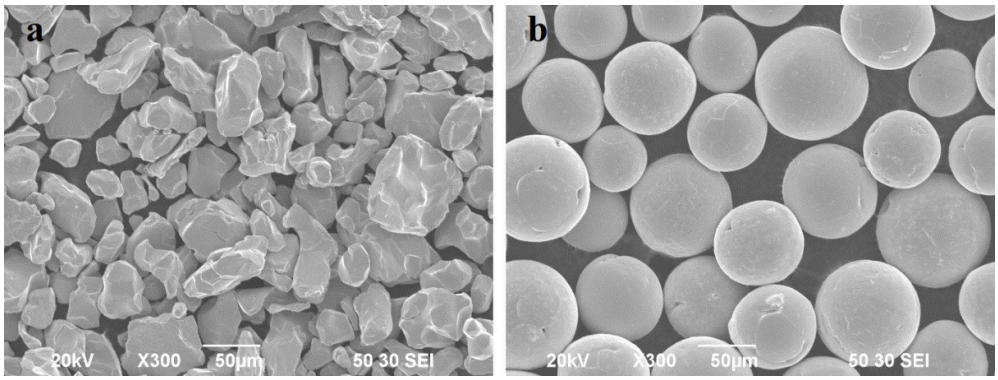

Figure 2. Particle morphology of (**a**) PM-M powder and (**b**) PMS-M99.9 powder.

2.2. LDED Equipment

LDED process was carried out on an installation equipped with a multimode ytterbium fiber laser IPG (IPG Photonics, Fryazino, Russia) with a power of 3000 W. The LDED equipment design is presented in Figure 3.

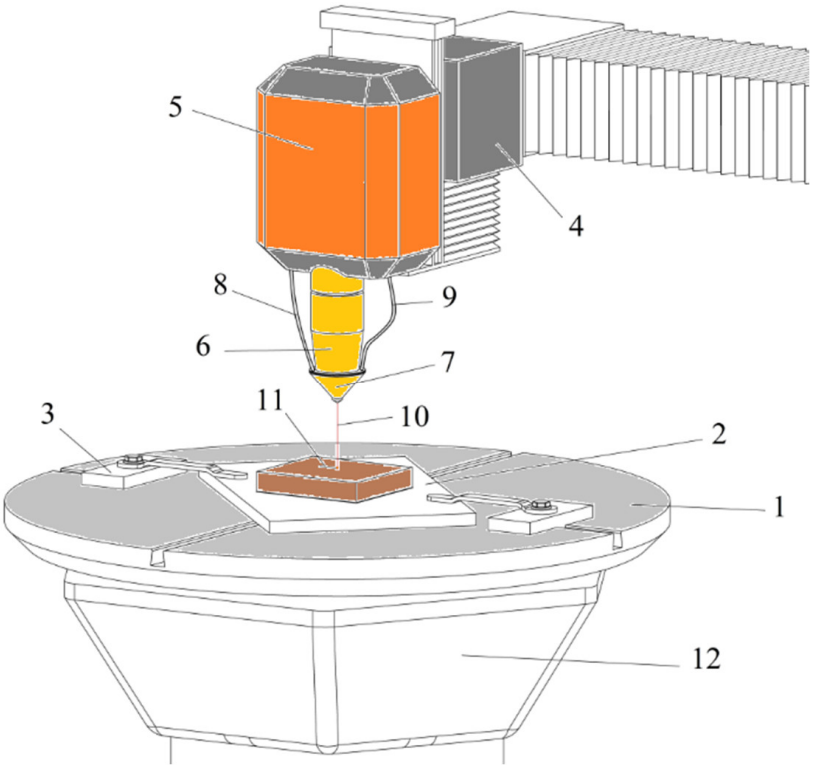

Figure 3. The design of LDED equipment: 1—table, 2—substrate, 3—mountings, 4—X–Y movement system, 5—laser module, 6—laser head, 7—coaxial nozzle, 8—powder feeding channels, 9—shield gas supply, 10—laser and powder flow jet, 11—deposited bead, and 12—X–Y–Z movement and rotation system.

The design of the installation included a working chamber with a size of 400 × 400 × 400 mm^3, a laser module, a module for preparing a gas–powder mixture with the ability to use powder fractions from 40 to 200 μm, a welding head (nozzle), a five-coordinate kinematic system based on linear motors and systems control with software that allows controlling the flow of the gas–powder mixture, optical units, and laser radiation in accordance with the motion paths created by the three-dimensional CAD model.

2.3. Sample Characterization

The microstructure and microrelief of the surface of the samples were studied using a Carl Zeiss Axio Observer D1m (Carl Zeiss Microscopy Ltd., Cambridge, UK) optical microscope and a PHENOM G2 PRO (SEM) with a built-in energy dispersive EDX analyzer (Thermo Fisher Scientific, Waltham, MA, USA).

Sample density was determined by hydrostatic weighing on a Mettler Toledo XP504 balance with an accuracy of 0.001 g/cm^3. Ethyl alcohol was used as the working fluid.

To analyze the microhardness, a Qness Q10A microhardness tester (Qness GmbH, Golling, Austria) was used with a maximum indenter load of 10 kilograms, which makes it possible to determine the hardness using the Vickers method with a measurement error HV = 0.01.

2.4. Fretting Wear Tests

Fretting wear is a mechanical wear of bodies in contact under conditions of small oscillatory movements. Wear resistance studies were carried out on a friction machine (Figure 4), which included electromagnetic vibration device 1 for testing of friction pairs during reciprocating movement of one of the samples. The loading system in the form of a balanced lever 4 transfers the normal load to the contact zone 5, which is regulated by loads of various masses. The systems for registration and control of experimental parameters include a sinusoidal signal amplifier (MMF VEB METRA) and a system for recording and monitoring parameters, a piezoelectric force sensor 3 with a resolution of Δ = 4 mN and a signal controller, and a laser displacement sensor 2 (D_{max} = ±250 μm, resolution Δ = 0.01 μm) with a controller.

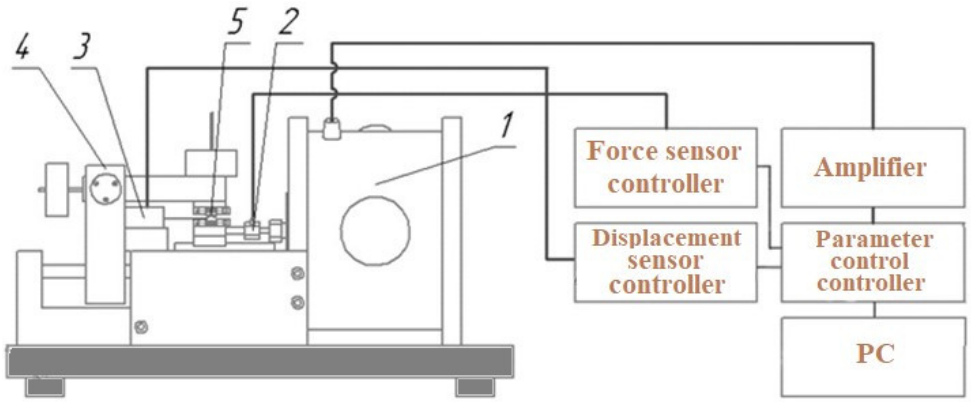

Figure 4. The scheme of the fretting wear test machine: 1—electromagnetic vibration device, 2—laser displacement sensor, 3—piezoelectric force sensor, 4—lever, and 5—contact zone.

The evaluation of tribological properties (friction coefficient and wear resistance) of the two types of laser-deposited molybdenum powder and brazed molybdenum layer was carried out on a friction machine in a reciprocating mode. The sphere/plane scheme was used as a model contact. The sphere was a ceramic wear-resistant ball with a diameter of ø10.6 mm made of Al_2O_3, while samples with a deposited molybdenum layer were used as a plane counterpart (Figure 5). The testing parameters are presented in Table 4.

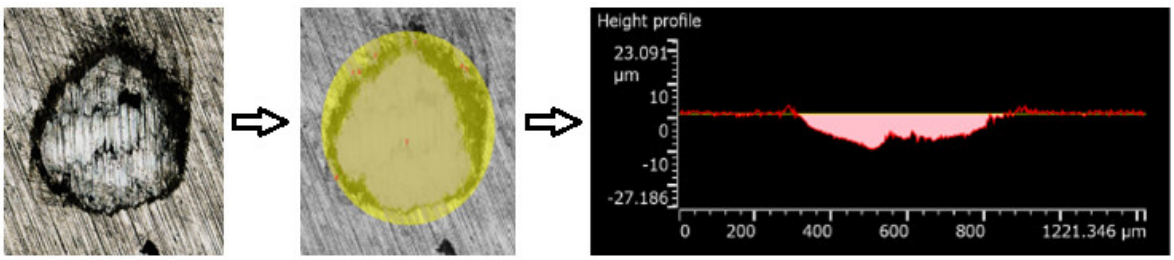

Figure 5. Stages of volumetric wear measuring after fretting wear tests.

Table 4. Fretting wear tests conditions.

Displacement D, μm	Frequency f, Hz	Load F_n, N	Number of cycles N	Atmosphere
100	20	5	10^5	Air

During the experiments, the values of the friction coefficients were recorded. Wear volume and wear damage were visually assessed using an Olympus LEXT OLS 5000 optical confocal microscope (Olympus, Tokyo, Japan). Comparative studies of wear resistance during fretting were carried out on samples of three types that imitate the protective layer of the "body" part, made according to traditional technology and LDED of powders PMS-M99.9 and PM-M with preferential parameters.

The procedure for measuring volumetric wear consists of the following steps (Figure 5):

1. Imaging wear spots on an optical confocal microscope;
2. Determining the area for wear measurement;
3. Setting the middle line, relative to which the volume will be calculated;
4. Calculating wear volume in special software.

2.5. Abrasive Wear Tests

The obtained samples with molybdenum coating were tested for abrasive wear on the Calowear machine (CSM Instruments, Peseux, Switzerland) according to the scheme in Figure 6.

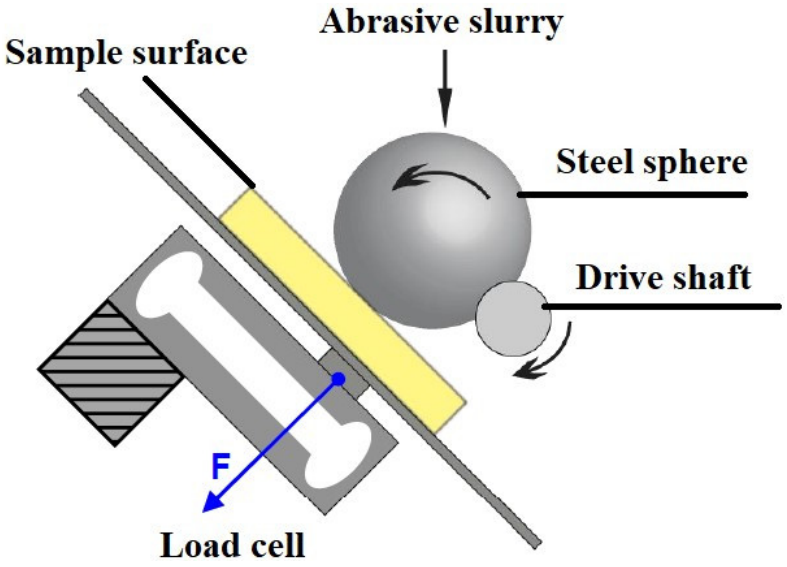

Figure 6. Abrasive wear test scheme.

The principle of measurement is based on forming a spherical crater on the surface of a specimen. A steel ball with a diameter of Ø25 mm in an abrasive medium rotates in contact with the surface of the specimen. An RDDM-grade diamond (15 carats) with a grain size of 0 to 1 μm was used as an abrasive. The normal force applied to the sample in the contact was 0.2 N. The rotation speed was 9.9 min^{-1}. The formed spherical crater was studied with an optical microscope, and wear volume V was calculated according to Equation (1).

$$V = \left(\frac{\pi d^4}{64R}\right) \quad (1)$$

where V is the wear volume in mm^3, R is the ball radius in mm, and d is the crater diameter in mm.

3. Results and Discussion

3.1. Determination of Preferential Parameters for LDED

The quality of the LDED process depends on a large number of operating parameters. By changing the operating parameters, it is possible to control the geometry and quality of the deposited beads and layers. The main variable parameters of the LDED process for single beads were powder consumption, laser radiation power, carrier gas consumption, and scanning strategy, scanning step, and step along the vertical axis for 3D objects.

The parameters of the LDED process were determined on the basis of the microstructure of the cross-section samples, their microhardness, and the geometry of single beads: width, height, and penetration depth. As a result, preferential parameters of LDED of molybdenum on 25L steel were found to be laser power P = 480 W, scanning speed V = 400 mm/min, powder consumption F_{pow} = 4 g/min, carrier gas F_{cgas} rate = 4 L/min, shielding gas F_{shgas} rate = 10 L/min and laser spot diameter = 1.2 mm. Figure 7 shows cross-sections of the obtained samples, while Table 5 presents the microhardness values of each sample. For the 3D objects, a hatch distance of 1.0 mm along with a vertical step Δz = 0.25 mm was chosen. The optical system provided a 1.2 mm laser spot with Gaussian distribution of energy within. The focal spot of the powder was 900 µm, and the working distance (the distance between the nozzle and substrate surface) was 11 mm.

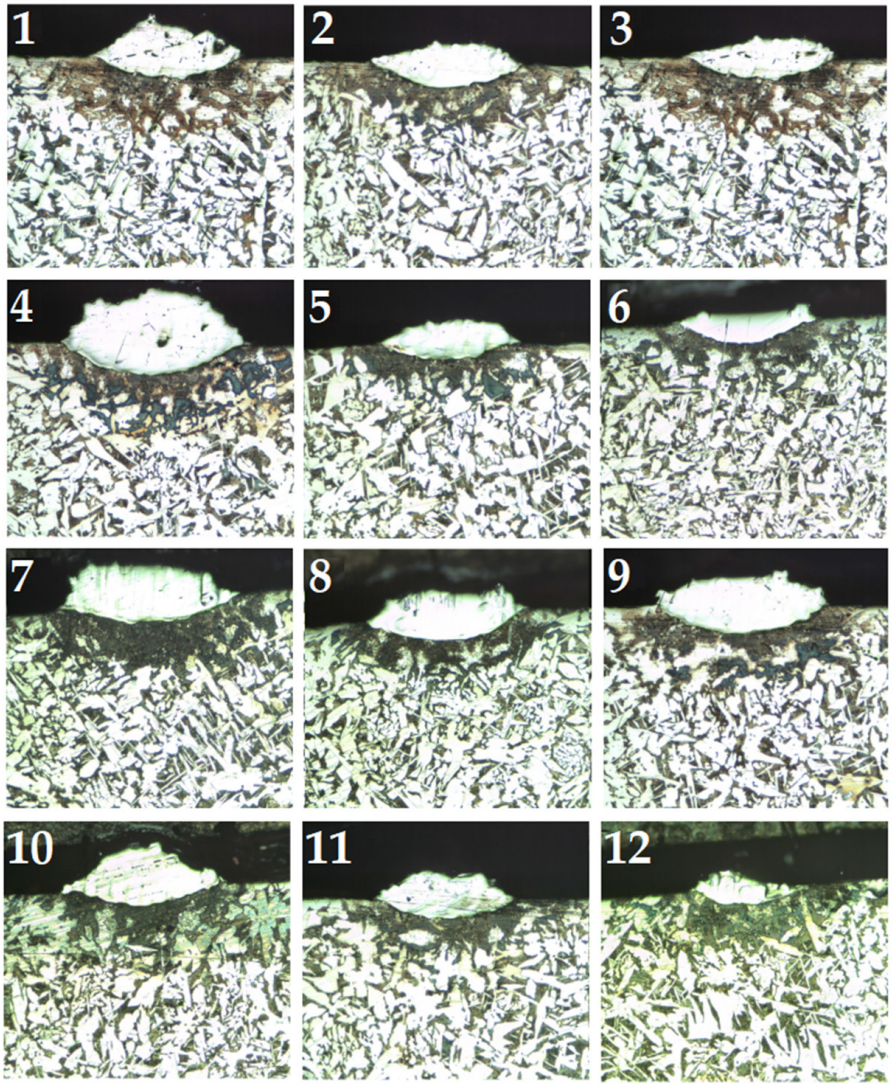

Figure 7. Cross-section images of single beads at different LDED parameters. Bead numbers are according to the Table 5.

Table 5. Hardness of the Mo coatings depending on the LDED working parameters.

Bead No.	Laser Power, W	Scanning Velocity, mm/min	Powder Feed Rate, g/min	Hardness, HV
1	360	200	2	248 ± 3
2	360	300	2	275 ± 12
3	360	400	2	503 ± 10
4	360	200	4	287 ± 15
5	360	300	4	300 ± 5
6	360	400	4	390 ± 16
7	480	200	4	278 ± 8
8	480	300	4	416 ± 24
9	480	400	4	465 ± 11
10	480	200	6	319 ± 26
11	480	300	6	336 ± 15
12	480	400	6	500 ± 30

The microstructure of the deposited layers from PM-M powder is full of pores (Figure 8a) while spherical powder resulted in homogeneous layers with a density from 9.8 to 10.0 g/cm^3 (Figure 8b).

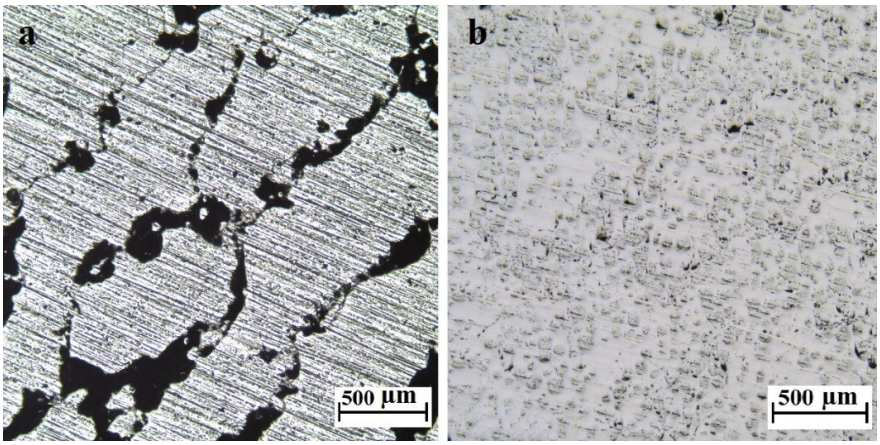

Figure 8. Microstructure of the cross-section of the deposited layers after LDED (×50): (**a**) powder PM-M; (**b**) powder PMS-M99.9.

The quality of the deposited coatings is greatly determined by the adhesion strength of the coating and the substrate. For this purpose, the microstructure of the boundary regions of the deposited layer of molybdenum and steel 25L was studied (Figure 9). Unlike for PMS-M99.9 powder, pores and transverse cracks were observed in the area of melt pool boundary in the deposited layer of PM-M powder on 25L steel substrate (Figures 9 and 10).

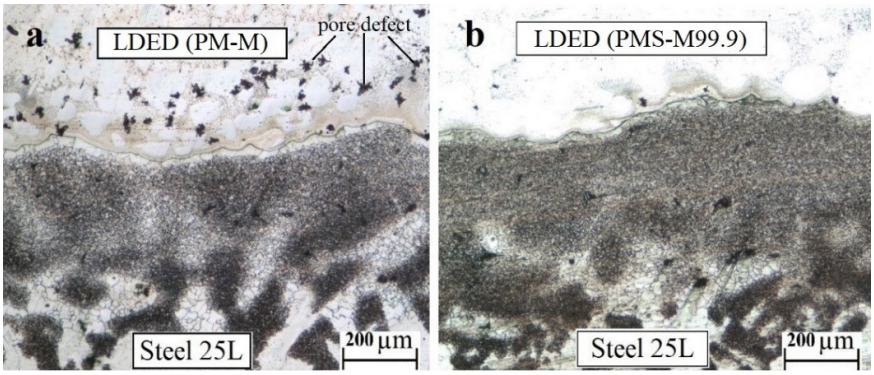

Figure 9. Microstructure of the Mo-steel boundary after LDED (×100): (**a**) powder PM-M; (**b**) powder PMS-M99.9.

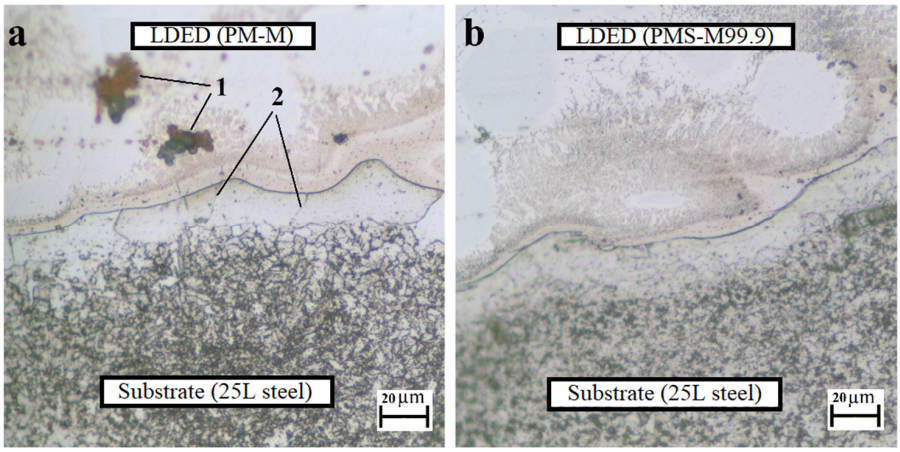

Figure 10. Microstructure of the Mo-steel boundary after LDED (×500): (**a**) PM-M powder with 1—pores and 2—cracks; (**b**) PMS-M99.9 powder.

SEM studies of the microstructure and distribution of elements of the transition layer showed a good metallurgical bond between the deposited layer and the steel base. This was confirmed by a gradual decrease in the percentage of Mo and an increase in the content of Fe in the direction from the surface of the deposited layer to the core (Table 6). The mutual diffusion of Mo and Fe on the Mo–steel boundary also supports this conclusion (Figures 11 and 12).

Table 6. Single EDX spectrum analysis in the Mo–steel boundary area (Figure 11b).

Spectrum No.	Elements Composition, wt.%			
	Si	Mn	Fe	Mo
1	-	-	-	100.00
2	-	-	-	100.00
3	0.3	-	29.68	70.02
4	0.35	-	38.79	60.86
5	-	-	-	100.00
6	-	-	-	100.00
7	0.41	0.24	49.20	50.15
8	0.43	0.34	49.52	49.71
9	0.75	0.54	98.59	0.12
10	0.63	0.45	98.81	0.11

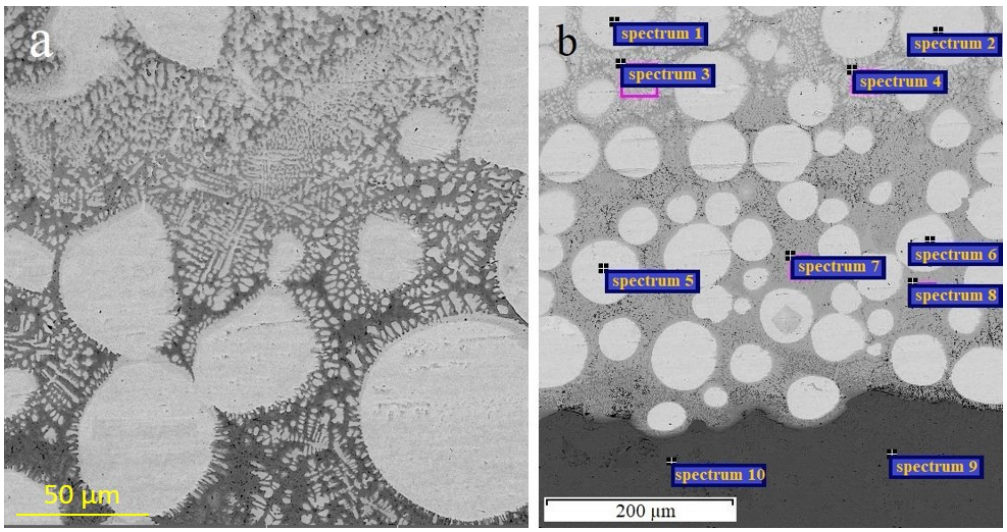

Figure 11. (**a**) Microstructure of the deposited Mo layer; (**b**) single EDX spectrum map.

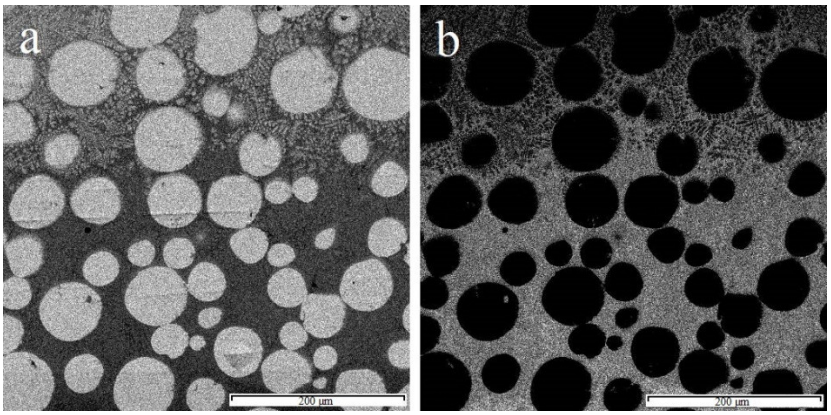

Figure 12. EDX distribution maps of (**a**) Mo and (**b**) Fe on the Mo–steel boundary.

Both round and dendrite crystals of Mo of different degrees of dispersion can be observed in Figure 11a. The dendrites were mostly columnar; however, in some cases, there were dendrites with axes of second order. Figure 12 shows elements distribution maps of Fe and Mo in the area of the melt pool boundary.

3.2. Fretting Wear

The results of the study, obtained by simulating the operation of a nominally fixed friction joint, make it possible to determine the qualitative and quantitative characteristics of the interface in terms of ensuring the integrity of the joint. Comparative studies of wear resistance during fretting showed that the coefficient of friction of all three coatings was almost the same at ~0.25 (Figure 13).

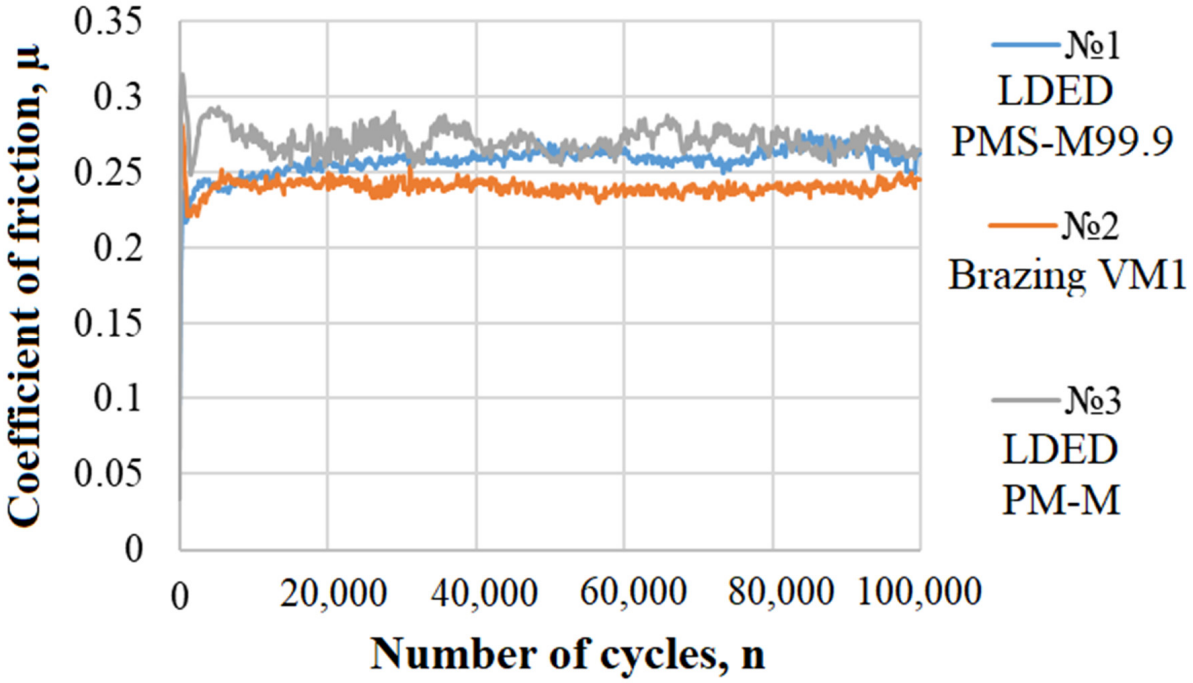

Figure 13. Dependence of friction coefficients on the number of cycles.

Figure 14 shows the results of destructive processes in the contact area of a nominally fixed friction joint during wear under fretting conditions (frequency = 20 Hz, load = 5 N, and number of cycles = 105).

It was revealed that, on the specimens made by brazing and LDED of PM-M powder, the value of volumetric wear (Table 7) was significantly higher compared to the molybdenum coating obtained by LDED of the PMS-M99.9 powder. This phenomenon can be

explained by the lower hardness of the molybdenum plate compared to the deposited molybdenum layers. The layer obtained by LDED of the PM-M powder also had significantly greater wear since the structure of the deposited molybdenum had defects in the form of pores and cracks.

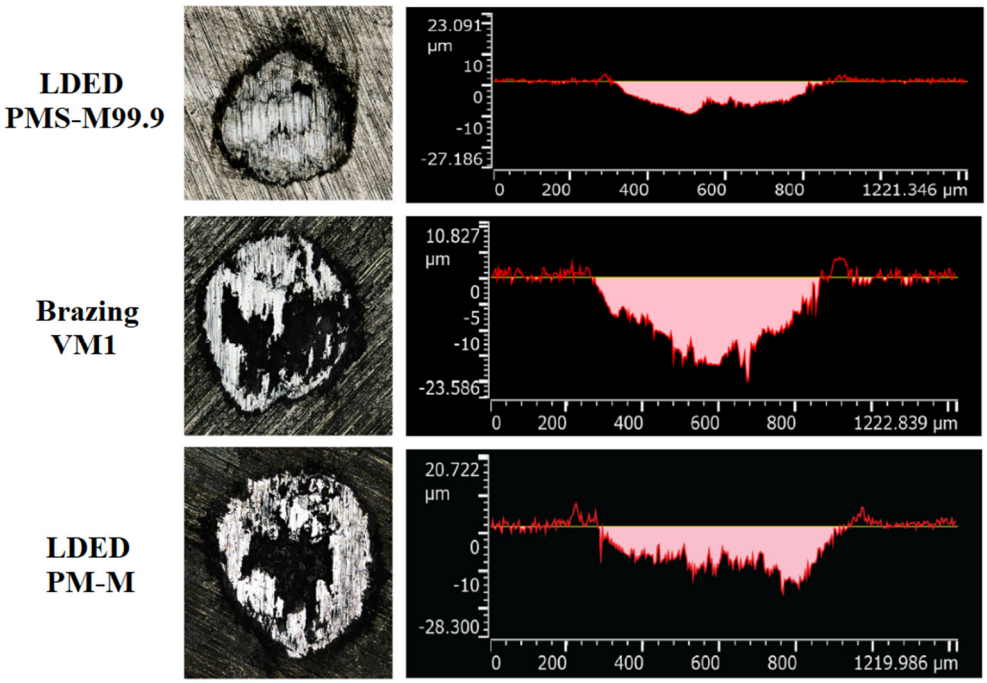

Figure 14. Contact area and the restored cross-section of the wear spot.

Table 7. Volumetric wear values of Mo layer after fretting wear tests (µm^3).

Test	LDED PMS-M99.9 Powder	Brazing VM1	LDED PM-M Powder
1	1,218,335	2,396,864	3,351,274
2	1,313,380	2,746,736	2,586,375
3	1,237,625	2,495,547	2,855,039

3.3. Abrasive Wear

Figures 15 and 16 present the results of comparative studies of abrasive wear tests of all three types of specimens: LDED of PM-M powder, LDED of PMS-M99.9 powder, and brazing.

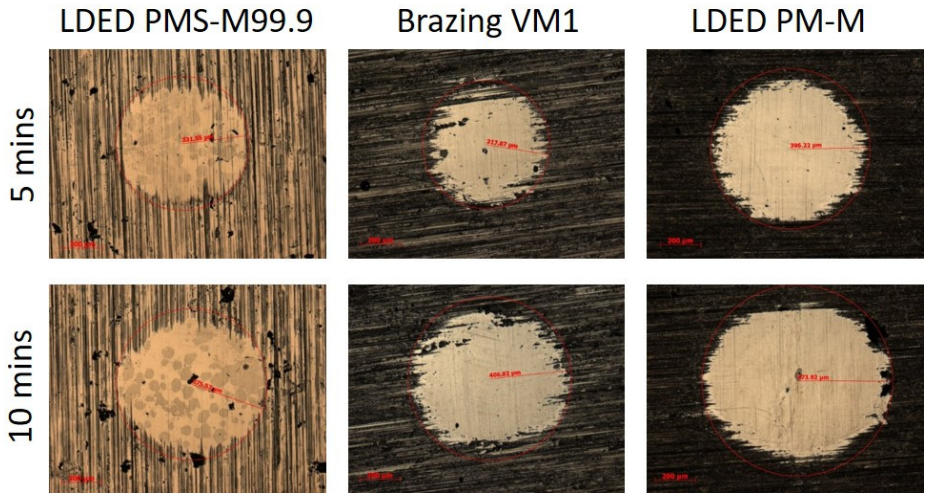

Figure 15. The development of destructive processes in the contact area during abrasive wear tests.

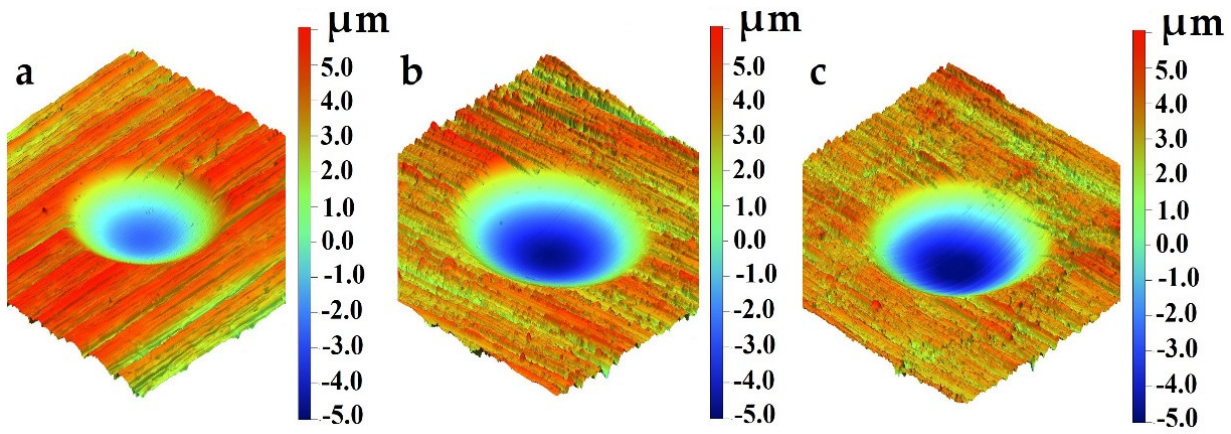

Figure 16. The 3D imaging of contact spot after 10 min of abrasive wear tests: (**a**) LDED of PMS-M99.9 powder, (**b**) brazing, and (**c**) LDED of PM-M powder.

The results of abrasive wear tests show that the volumetric wear of the PMS-M99.9 LDED coating was more than 2.5 times lower than that of PM-M powder (Figure 17, Table 8). The poor wear resistance of the LDED PM-M coating is explained by the presence of microstructural defects due to the irregular shape of particles of the raw material. Moreover, being harder, the PMS-M99.9 LDED coating outperformed the brazed Mo coating.

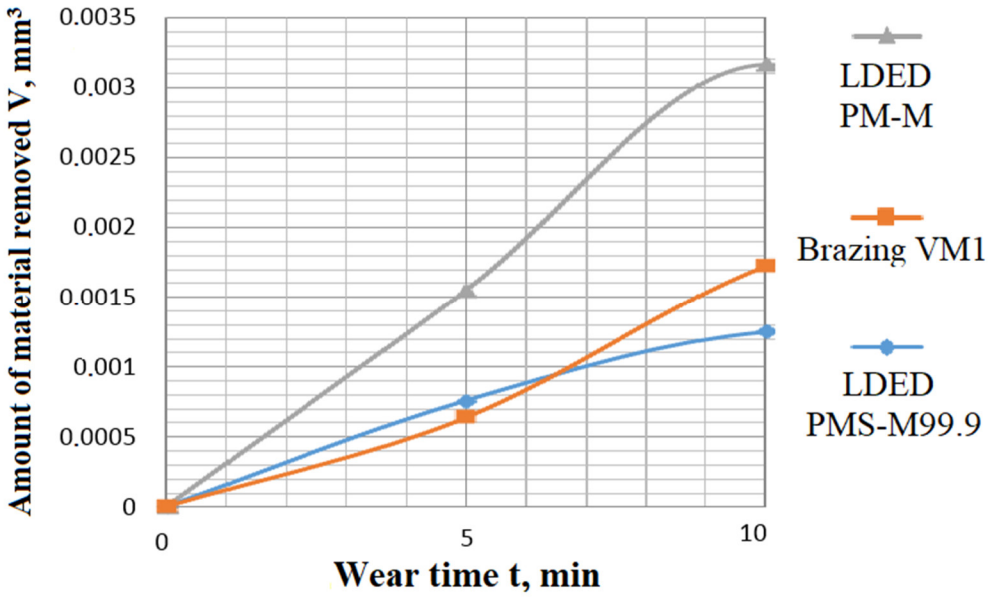

Figure 17. The dependence of the volume of material removed from the wear time.

Table 8. Volumetric wear values of Mo layer after abrasive wear tests.

	Volumetric Wear of Mo Layer (mm^3)		
Test Duration, min	**LDED PMS-M99.9 Powder**	**Brazing VM1**	**LDED PM-M Powder**
5	0.000759	0.000635	0.001548
10	0.001249	0.001722	0.003169

Thus, the "body" part made by LDED of the PMS-M99.9 spherical powder provided better performance properties compared to the traditional manufacturing technology.

4. Conclusions

Studying the process of LDED of molybdenum powders PM-M of irregular shape and PMS-M99.9 of spherical shape showed that PMS-M99.9 is suitable for the LDED technology and provides depositing stable layers with homogeneous microstructure and density in the range 9.8–10.0 g/cm^3. LDED of powder with irregularly shaped particles resulted in microstructural defects such as pores and cracks.

Preferential parameters of LDED of PMS-M99.9 including laser power P = 480 W, scanning speed V = 400 mm/min, powder consumption F_{pow} = 4 g/min, carrier gas F_{cgas} rate = 4 L/min, shielding gas F_{shgas} rate = 10 L/min, hatch distance = 1 mm, vertical step Δz = 0.25 mm, and laser spot diameter = 1.2 mm provided Mo layers with a homogeneous flawless microstructure and a strong metallurgical bond with substrate, as confirmed by mutual diffusion of Mo and Fe on the Mo–steel boundary. Moreover, LDED improves hardness, abrasion, and fretting wear resistance.

Comparative abrasive wear tests for 10 min showed that the wear resistance of the LDED of PMS-M99.9 powder was 2.54 times higher than PM-M powder and 1.38 higher than brazed molybdenum.

Comparative fretting wear tests showed that the friction coefficient of all three types of specimens had the same value of ~0.25. The lowest volumetric wear was measured for the LDED PMS-M99.9 powder.

Author Contributions: Conceptualization, T.T., A.S. and S.N.G.; methodology, T.T. and A.S.; software, A.S.M. and M.V.; validation, A.S., T.T. and P.P.; formal analysis, T.T., A.S. and P.P.; investigation, T.T. and A.S.; resources, S.N.G.; data curation, A.S.M. and M.V.; writing—original draft preparation, T.T. and A.S.; writing—review and editing, T.T. and P.P.; visualization, P.P. and A.S.; supervision, S.N.G.; project administration, S.N.G.; funding acquisition, S.N.G. All authors have read and agreed to the published version of the manuscript.

Funding: This work was funded by the state assignment of the Ministry of Science and Higher Education of the Russian Federation, Project No. FSFS-2021-0006.

Data Availability Statement: Not applicable.

Acknowledgments: The study was carried out on the equipment of the Center of Collective Use "State Engineering Center" of MSUT "STANKIN" supported by the Ministry of Higher Education of the Russian Federation (project 075-15-2021-695 from 26 July 2021, unique identifier RF 2296.61321X0013).

Conflicts of Interest: The authors declare no conflict of interest.

References

1. Pathak, S.; Saha, G.C. Development of Sustainable Cold Spray Coatings and 3D Additive Manufacturing Components for Repair/Manufacturing Applications: A Critical Review. *Coatings* **2017**, *7*, 122. [CrossRef]
2. Sova, A.; Okunkova, A.; Grigoriev, S.; Smurov, I. Velocity of the particles accelerated by a cold spray micronozzle: Experimental measurements and numerical simulation. *J. Therm. Spray Technol.* **2013**, *22*, 75–80. [CrossRef]
3. Sova, A.; Grigoriev, S.; Okunkova, A.; Smurov, I. Potential of cold gas dynamic spray as additive manufacturing technology. *Int. J. Adv. Manuf. Technol.* **2013**, *69*, 2269–2278. [CrossRef]
4. Kotoban, D.; Grigoriev, S.; Okunkova, A.; Sova, A. Influence of a shape of single track on deposition efficiency of 316L stainless steel powder in cold spray. *Surf. Coat. Technol.* **2017**, *309*, 951–958. [CrossRef]
5. Tarasova, T.V. Prospects for the use of laser radiation to improve the wear resistance of corrosion-resistant steels. *Met. Sci. Heat Treat. Met.* **2010**, *6*, 54–58.
6. ASTMF2792-12a. Standard Terminology for Additive Manufacturing Technologies. ASTM International: West Conshohocken, PA, USA, 2012.
7. ISO/ASTM 52900:2015. Additive Manufacturing—General Principles—Terminology. ISO/ASTM International: Geneva, Switzerland, 2015; p. 19. Available online: https://www.sis.se/api/document/preview/919975/ (accessed on 15 August 2015).
8. Gusarov, A.V.; Grigoriev, S.N.; Volosova, M.A.; Melnik, Y.A.; Laskin, A.; Kotoban, D.V.; Okunkova, A.A. On productivity of laser additive manufacturing. *J. Mater. Process. Technol.* **2018**, *261*, 213–232. [CrossRef]
9. Grigoriev, S.N.; Tarasova, T.V. Possibilities of the technology of additive production for making complex-shape parts and depositing functional coatings from metallic powders. *Met. Sci. Heat Treat.* **2016**, *57*, 579–584. [CrossRef]

10. Khmyrov, R.S.; Grigoriev, S.N.; Okunkova, A.A.; Gusarov, A.V. On the possibility of selective laser melting of quartz glass. *Phys. Procedia* **2014**, *56*, 345–356. [CrossRef]
11. Khmyrov, R.S.; Protasov, C.E.; Grigoriev, S.N.; Gusarov, A.V. Crack-free selective laser melting of silica glass: Single beads and monolayers on the substrate of the same material. *Int. J. Adv. Manuf. Technol.* **2016**, *85*, 1461–1469. [CrossRef]
12. Doubenskaia, M.; Pavlov, M.; Grigoriev, S.N.; Smurov, I. Definition of brightness temperature and restoration of true temperature in laser cladding using infrared camera. *Surf. Coat. Technol.* **2013**, *220*, 244–247. [CrossRef]
13. Doubenskaia, M.; Pavlov, M.; Grigoriev, S.N.; Tikhonova, E.; Smurov, I. Comprehensive Optical Monitoring of Selective Laser Melting. *J. Laser Micro Nanoeng.* **2012**, *7*, 236–243. [CrossRef]
14. Grigoriev, S.N.; Teleshevskii, V.I. Measurement problems in technological shaping processes. *Meas. Tech.* **2011**, *54*, 744–749. [CrossRef]
15. Smurov, I.; Doubenskaia, M.; Grigoriev, S.N.; Nazarov, A. Optical Monitoring in Laser Cladding of Ti6Al4V. *J. Therm. Spray Tech.* **2012**, *21*, 1257–1362. [CrossRef]
16. Ding, Y.; Bi, W.; Zhong, C.; Wu, T.; Gui, W. A Comparative Study on Microstructure and Properties of Ultra-High-Speed Laser Cladding and Traditional Laser Cladding of Inconel625 Coatings. *Materials* **2022**, *15*, 6400. [CrossRef]
17. Parthasarathy, T.; Mendiratta, M.; Dimiduk, D. Oxidation mechanisms in Mo-reinforced Mo_5SiB_2(T2)–Mo_3Si alloys. *Acta Mater.* **2002**, *50*, 1857–1868. [CrossRef]
18. Dimiduk, D.M.; Perepezko, J.H. Mo-Si-B Alloys: Developing a Revolutionary Turbine-Engine Material. *MRS Bull.* **2003**, *28*, 639–645. [CrossRef]
19. Li, Q.; Wang, C.; Li, Z.; Qu, Y.; Li, X. Comparative Study on the Surface Remelting of Mo-Si-B Alloys with Laser and Electron Beam. *Materials* **2022**, *15*, 6223. [CrossRef]
20. Zhao, J.-C.; Westbrook, J.H. Ultrahigh-Temperature Materials for Jet Engines. *MRS Bull.* **2003**, *28*, 622–630. [CrossRef]
21. Lemberg, J.A.; Ritchie, R.O. Mo-Si-B Alloys for Ultrahigh-Temperature Structural Applications. *Adv. Mater.* **2012**, *24*, 3445–3480. [CrossRef]
22. Bewlay, B.P.; Jackson, M.R.; Subramanian, P.; Zhao, J.-C. A review of very-high-temperature Nb-silicide-based composites. *Metall. Mater. Trans. A* **2003**, *34*, 2043–2052. [CrossRef]
23. Perepezko, J.H. The Hotter the Engine, the Better. *Science* **2009**, *326*, 1068–1069. [CrossRef] [PubMed]
24. Wang, F.; Shan, A.; Dong, X.; Wu, J. Microstructure and oxidation resistance of laser-remelted Mo–Si–B alloy. *Scr. Mater.* **2007**, *56*, 737–740. [CrossRef]
25. Makineni, S.; Kini, A.; Jägle, E.; Springer, H.; Raabe, D.; Gault, B. Synthesis and stabilization of a new phase regime in a Mo-Si-B based alloy by laser-based additive manufacturing. *Acta Mater.* **2018**, *151*, 31–40. [CrossRef]
26. Schmelzer, J.; Rittinghaus, S.-K.; Weisheit, A.; Stobik, M.; Paulus, J.; Gruber, K.; Wessel, E.; Heinze, C.; Krüger, M. Printability of gas atomized Mo-Si-B powders by laser metal deposition. *Int. J. Refract. Met. Hard Mater.* **2018**, *78*, 123–126. [CrossRef]
27. Zhou, W.; Sun, X.; Tsunoda, K.; Kikuchi, K.; Nomura, N.; Yoshimi, K.; Kawasaki, A. Powder fabrication and laser additive manufacturing of MoSiBTiC alloy. *Intermetallics* **2019**, *104*, 33–42. [CrossRef]
28. Zhou, W.; Tsunoda, K.; Nomura, N.; Yoshimi, K. Effect of hot isostatic pressing on the microstructure and fracture toughness of laser additive-manufactured MoSiBTiC multiphase alloy. *Mater. Des.* **2020**, *196*, 10913. [CrossRef]
29. Fichtner, D.; Schmelzer, J.; Yang, W.; Heinze, C.; Krüger, M. Additive manufacturing of a near-eutectic Mo–Si–B alloy: Processing and resulting properties. *Intermetallics* **2020**, *128*, 107025. [CrossRef]
30. Guo, Z.; Han, R.; Li, Y.; Zhu, Y.; Zhang, B.; Zhang, H. Mo-Si-B Alloy Formed by Optional Laser Melting Process. *Int. J. Anal. Chem.* **2022**, *2022*, 4996265. [CrossRef]
31. Metel, A.S.; Tarasova, T.; Skorobogatov, A.; Podrabinnik, P.; Melnik, Y.; Grigoriev, S.N. Feasibility of Production of Multimaterial Metal Objects by Laser-Directed Energy Deposition. *Metals* **2022**, *12*, 1566. [CrossRef]
32. Yan, A.; Atif, A.M.; Wang, X.; Lan, T.; Wang, Z. The Microstructure and Cracking Behaviors of Pure Molybdenum Fabricated by Selective Laser Melting. *Materials* **2022**, *15*, 6230. [CrossRef]
33. Wei, C.; Zhang, Z.; Cheng, D.; Sun, Z.; Zhu, M.; Li, L. An overview of laser-based multiple metallic material additive manu facturing: From macro- to micro-scales. *Int. J. Extrem. Manuf.* **2021**, *3*, 012003. [CrossRef]
34. Chen, Y.; Peng, X.; Kong, L.; Dong, G.; Remani, A.; Leach, R. Defect inspection technologies for additive manufacturing. *Int. J. Extrem. Manuf.* **2021**, *3*, 022002. [CrossRef]